Supplement of

Do large-scale wind farms affect air quality forecast? Modeling evidence in Northern China

Authors:

Si Li[1,3], Tao Huang[1]*, Jingyue Mo[4], Jixiang Li[1], Xiaodong Zhang[1], Jiao Du[1], Shu Tao[2], Junfeng Liu[2], Wanyanhan Jiang[1], Lulu Lian[1], Hong Gao[1], Xiaoxuan Mao[1], Yuan Zhao[2], Jianmin Ma[2, 1]*

Affiliations:

[1]Key Laboratory for Environmental Pollution Prediction and Control, Gansu Province; College of Earth and Environmental Sciences, Lanzhou University, Lanzhou 730000, P. R. China

[2]Laboratory for Earth Surface Processes, College of Urban and Environmental Sciences, Peking University, Beijing 100871, P. R. China

[3]College of Atmospheric Sciences, Lanzhou University, Lanzhou 730000, P. R. China

[4]Chinese Academy of Meteorological Sciences, Beijing 100000, P. R. China

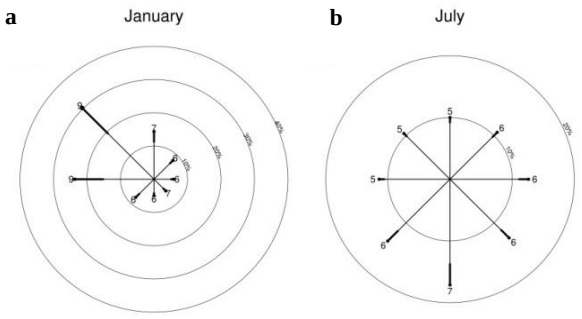

Figure S1. Wind rose diagrams over the model domain at the hub height (**Fig. 1** in main text) averaged over January (a) and July (b), 2016, respectively.

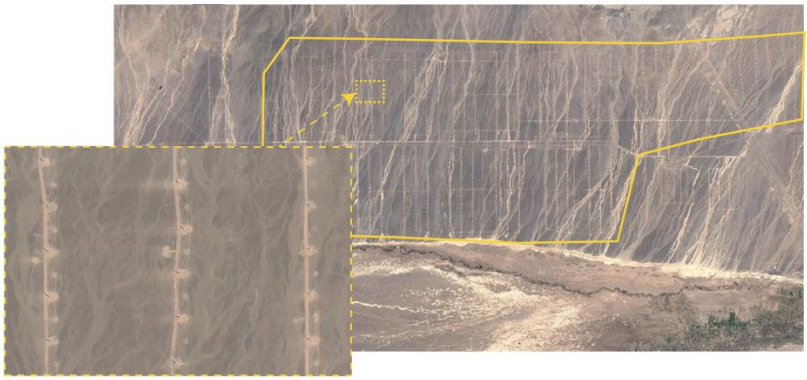

Figure S2. Location of wind farms and wind turbines. The satellite photo was taken from ©Google.

Text 1. Model evaluation

Text 1.1 $PM_{2.5}$

To evaluate the performance of model simulations, WRF-Chem simulated $PM_{2.5}$ concentrations were compared with the observations at five monitoring stations in January and July 2016. The locations of these 5 stations are listed in **Table S3**. Statistical metrics were employed to evaluate modeling results, including correlation coefficient (R), mean bias (MB), normalized mean bias (NMB), mean gross error (MGE), normalized mean gross error (NMGE), fraction of model predictions (FAC2) within $0.5 \leq S_i/O_i \leq 2.0$, where S_i is the simulated result and O_i is measured data, FAC5 (the same as FAC2 but for $0.2 \leq S_i/O_i \leq 5.0$), FAC10 (the same as FAC2, but for $0.1 \leq S_i/O_i \leq 10.0$). The statistical metrics are presented in **Tables S4** and **S5** for January and July, respectively. The expression of these statistical parameters are defined below:

$$\mathrm{MB} = \frac{1}{\mathrm{N}} \sum_1^N (S_i - O_i) \quad \text{(S1)}$$

$$\mathrm{NMB} = \frac{\sum_1^N (S_i - O_i)}{\sum_1^N O_i} \quad \text{(S2)}$$

$$\mathrm{MGE} = 1/\mathrm{N} \sum_1^N |S_i - O_i| \quad \text{(S3)}$$

$$\mathrm{NMGE} = \frac{\sum_1^N |S_i - O_i|}{\sum_1^N O_i} \quad \text{(S4)}$$

Figure S3 shows the hourly time series of modeled $PM_{2.5}$ concentrations from the BASE scenario simulations and observation in January and July. In general, the model captures temporal variation in January and July, with the correlation coefficient of 0.59 in January and 0.59 in July, respectively. However, the model underestimates $PM_{2.5}$ levels as compared to the measured values, characterized by negative mean bias with the MB of -13.3 μg m^{-3} (-38%) in January and -6.13 μg m^{-3} (-16%) in July, respectively. WRF model performance differs in different locations. As shown in **Tables S4** and **S5**, the normalized mean bias (NMB) in January ranges from -4.49% at the Siping (SP) station to -78.76% at the Hinggan (HG) station in January and from -3.29% at the Beijing (BJ) site to -54.07% at HG, suggesting marked underestimation of $PM_{2.5}$ at the HG in both January and July. Compared to January, the WRF-Chem shows slightly better performance in July, with the NMB and NMGE at -16.03% and 56.1% relative to the NMB and NMGE in January at -37.61% and 64.1%.

Figure S4 is a scatter plot for hourly $PM_{2.5}$ concentrations (μg m^{-3}) between model simulation and monitoring results at the five sampling stations (**Table S3**). Most scatter points are within the 0.2:1 line and 5:1 line, with the FAC5 of 0.82 and 0.84 in January and July, respectively. As shown, the WRF-Chem tends to yield better predictions to $PM_{2.5}$ at relatively low pollutant levels. **Figure S5** further shows correlation diagrams between predicted and sampled $PM_{2.5}$ concentrations at each sampling station**.**

Due to the uncertainty of the physical and chemical processes in model and the emissions inventory, the model still exhibit uncertainties in predicted $PM_{2.5}$ concentrations. Nevertheless, our model evaluation results indicate that the WRF-Chem is capable of predicting the diurnal and daily variations of $PM_{2.5}$ in the model domain.

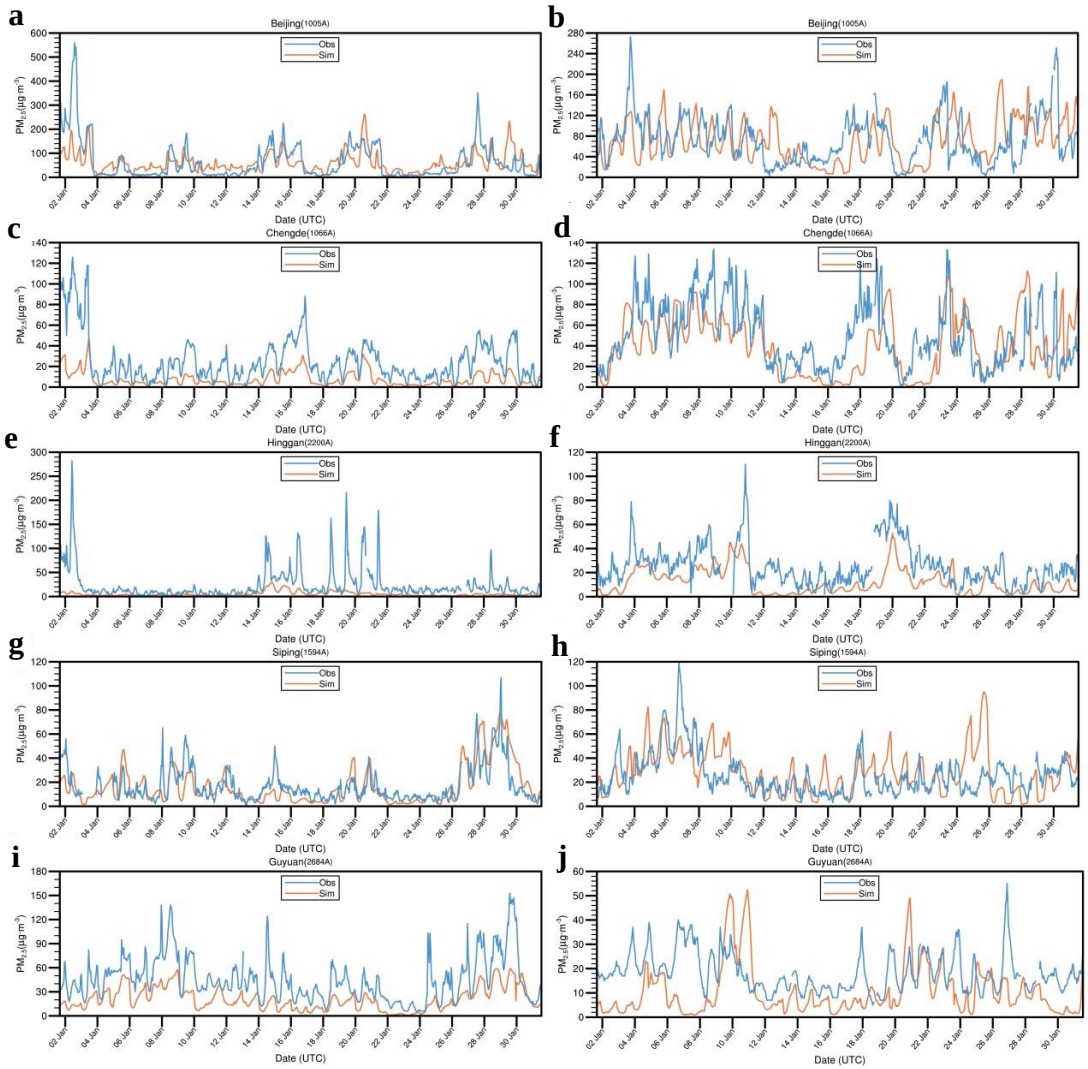

Figure S3. Hourly time series of modeled and observed $PM_{2.5}$ at Beijing (a), Chengde (c), Hinggan (e), Siping (g), Guyuan (i) in January (left panel), and July (right panel, b, d, f, h, j) 2016. The orange solid line and blue solid line represent the simulated and sampled data, respectively.

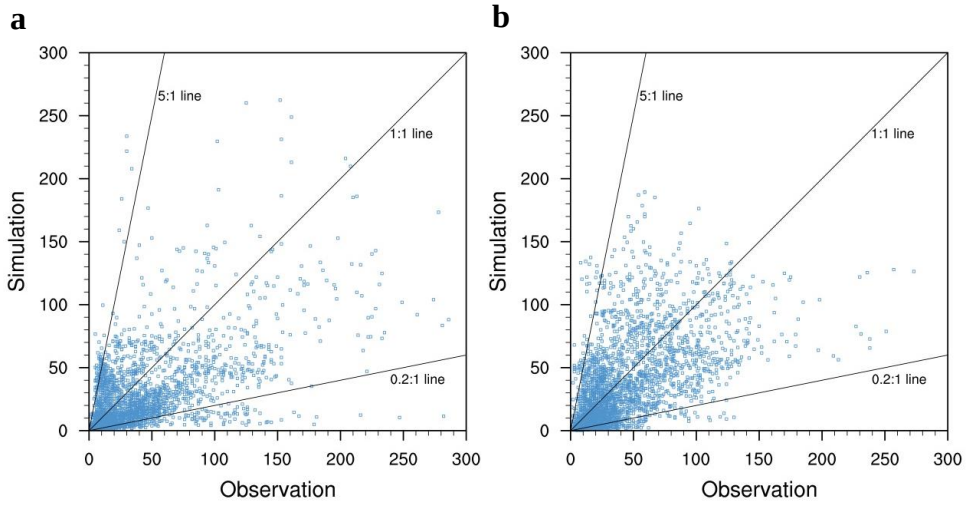

Figure S4. Scatter plots of hourly $PM_{2.5}$ concentrations (μg m^{-3}) between model and observation at five stations (**Table S3**) in January **(a)** and July **(b)** 2016. Three solid black lines denote 1:1 line and the boundaries where simulated concentrations are 5 and 0.2 times of measured data.

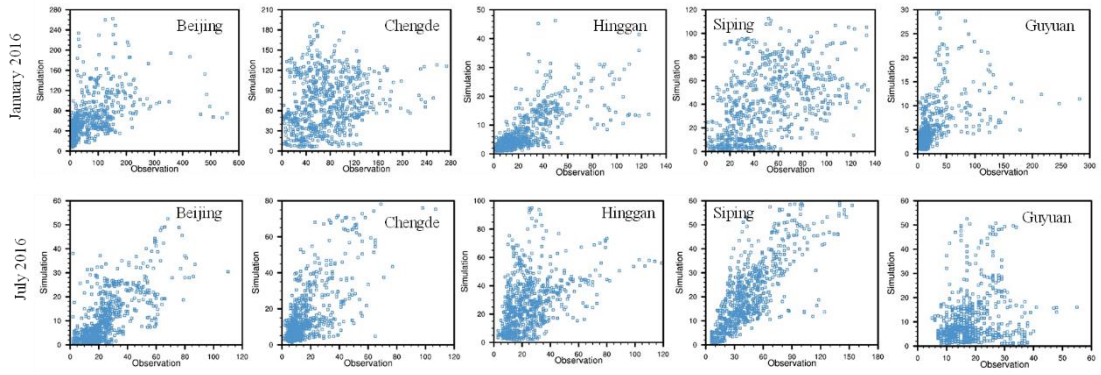

Figure S5. Scatter plot of hourly $PM_{2.5}$ concentrations between model and measurement at each selected sampling station (**Table S3**) in January (upper panel) and July (lower panel) 2016.

Text 1.2 Air temperature and wind speed

Figure S6 shows WRF modeled and measured hourly air temperatures (°C) in January (left panel) and July (right panel) 2016 at the five selected met observational stations located in the inner domain, including Beijing, Chengde, Hinggan, Siping, and Guyuan. Overall, the WRF model captures diurnal and daily changes in air temperatures. **Figure S7** are correlation diagrams between simulated and observed air temperatures in January (left panel) and July (right panel) 2016. It is evident that the agreement between modeled and measured air temperatures is good. The correlation coefficients between simulated and observed temperatures in January range from 0.79 to 0.95 for the five stations with the mean R of 0.87 over the five stations (**Table S6**). Lower correlation coefficients between the modeled and measured air temperatures occurred in July with

R ranging from 0.65 to 0.82 at the 5 stations and the mean R of 0.81 over the 5 sites (**Table S7**). In January, the WRF model slightly underestimated mean air temperatures averaged over the 5 stations with the mean bias at -3.7 ^{o}C with the largest mean bias at the Beijing observational station (-5.19 ^{o}C). In July, while we observed relatively lower correlation coefficients between the modeled and observed temperatures, the mean bias is smaller at all 5 stations, ranging from -2.36 in Chengde to 2.37 in Guyuan, with the mean MB at 0.21 over the five stations.

The WRF modeled hourly wind speeds at the 10 m height at the five observational stations are weakly correlated with the measured wind speeds. The mean R between simulated and observed wind speeds over the 5 stations is 0.48 in January (**Table S8**) and 0.26 (**Table S9**) in July 2016, respectively. The weak correlations were likely attributed, to some extent, to local turbulent activities in hourly wind speeds, causing the fluctuations and deviations from the hourly mean wind speed. Whereas, the WRF predicted wind speeds are, in reality, the mean winds averaged over the 10 km ×10 km grid cell, which filter out, to a large degree, the local turbulence induced wind speed fluctuations. Instead of presenting the turbulence disturbed hourly wind speeds, **Figure S8** show daily averaged wind speeds from WRF prediction and measurements at the 5 sites during January and July 2016. WRF modeled wind speeds captured, to some extent, the daily variations of the measured wind speeds at the 5 observation stations in both January and July but tended to overestimated the wind speeds, except in Beijing and Guyuan in January and Guyuan in July. Such overestimations can be also identified in **Figure S9** which is a correlation diagram between WRF simulated and measured wind speeds over the 5 observation stations in January and July. The detailed statistics between modeled and measured wind speeds are presented in **Table S10** (January 2016) and **S11** (July 2016). These statistics indicate that, overall, the WRF predicted wind speeds agree reasonably well with the measured data, particularly in January. The relatively lower predictability of summer (July) wind speeds was again related to local-scale circulations induced by non-uniform surface heating and cooling often occurring in the summertime.

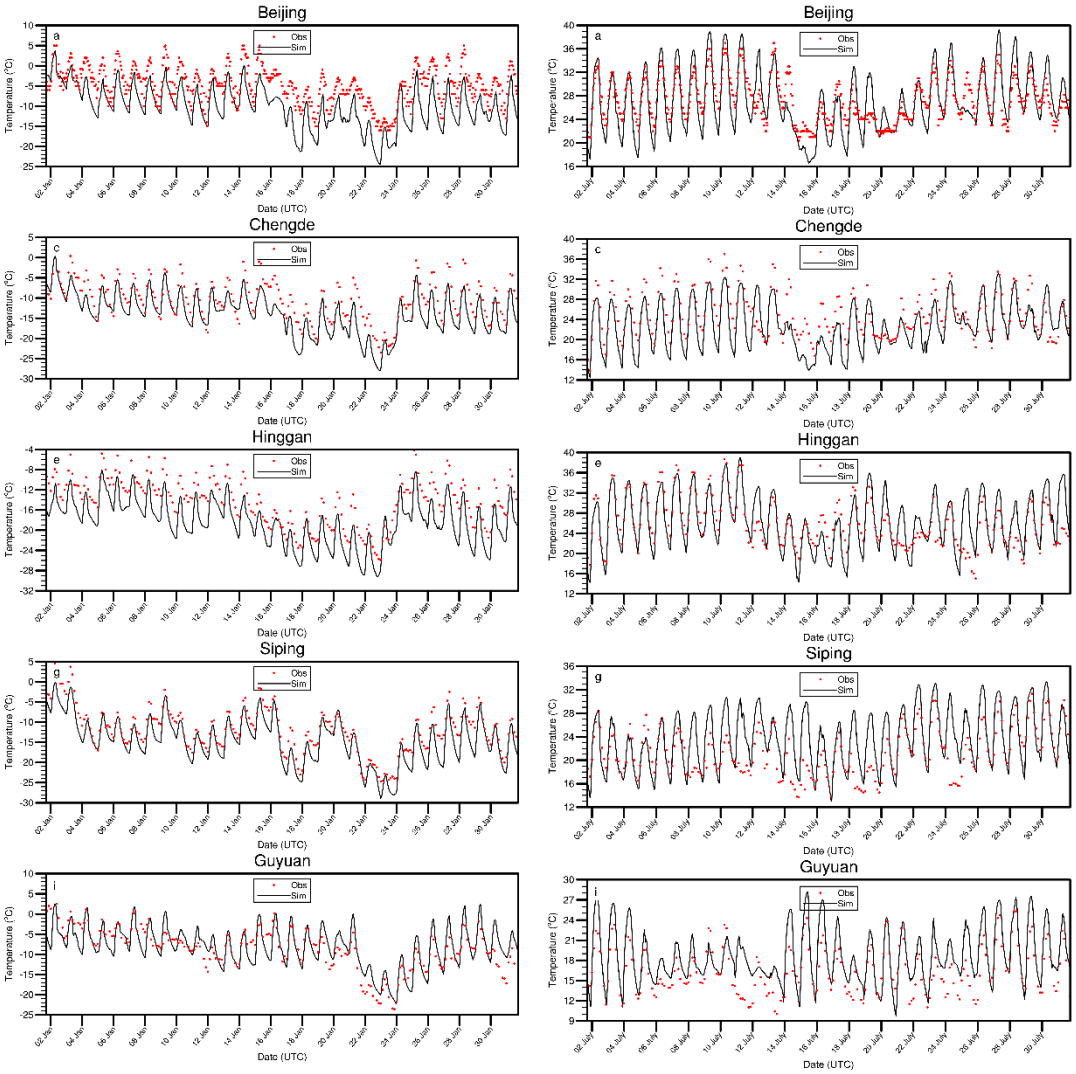

Figure S6. Hourly time series of modeled and measured surface air temperatures in January (left panel) and July (right panel) 2016 at five meteorological observation stations, including Beijing, Chengde, Hinggan, Siping, and Guyuan.

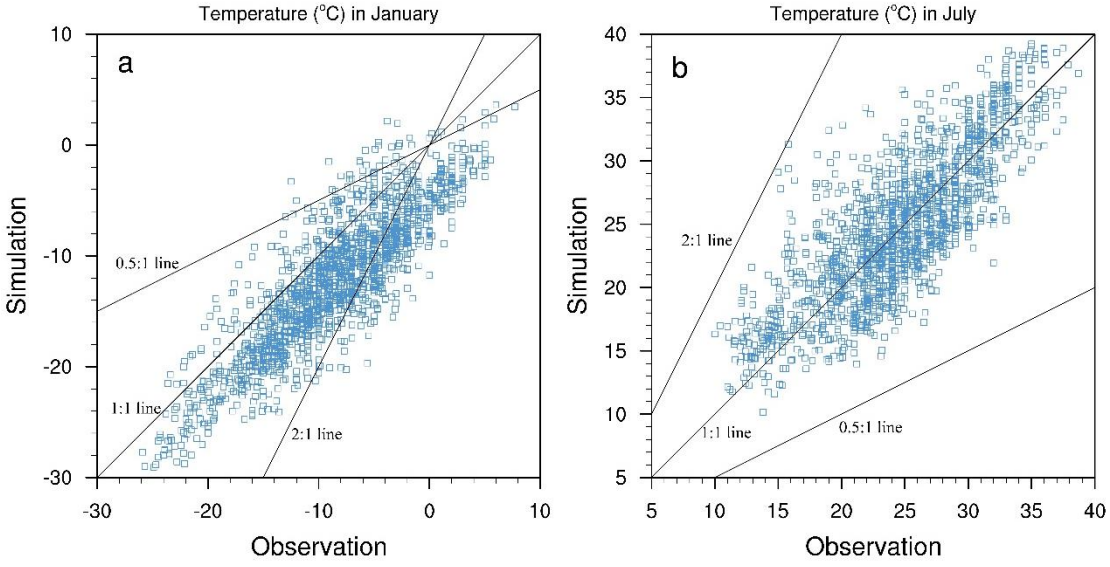

Figure S7. Scatter plots of hourly surface temperatures between model and observation at five observational stations in January **(a)** and July **(b)** 2016. Three solid black lines denote 1:1 and the boundaries where simulated temperatures are 0.5 and 2 time of measured data.

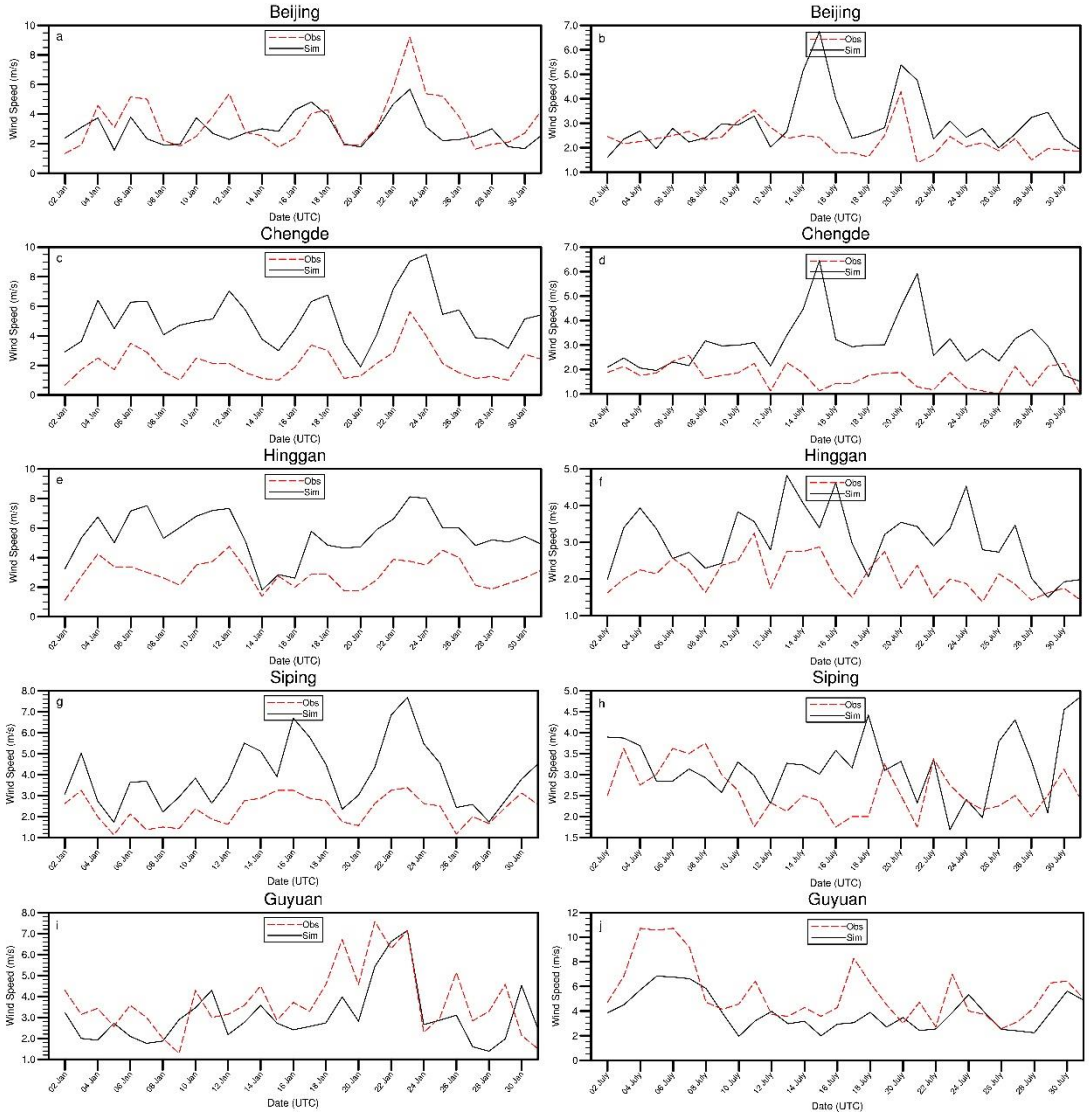

Figure S8. Daily time series of modeled and measured wind speeds at the 10 m height in January (left panel) and July (right panel) 2016 at five meteorological observation stations, including Beijing, Chengde, Hinggan, Siping, and Guyuan.

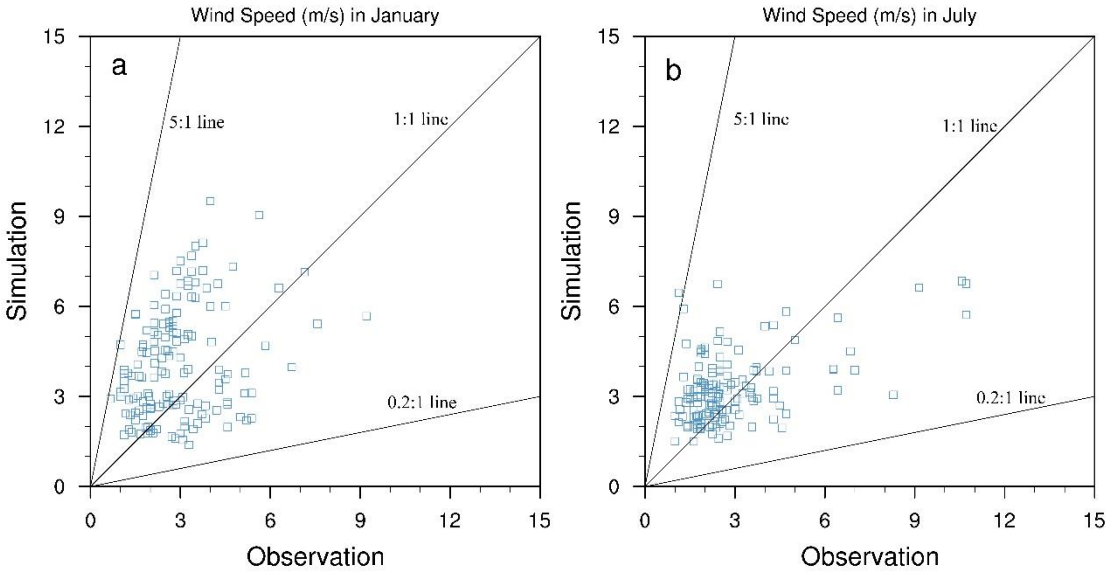

Figure S9. Scatter plots of daily wind speeds at the 10 m height between model and observation for five observational stations in January **(a)** and July **(b)** 2016. Three solid black lines denote 1:1 and the boundaries where simulated wind speeds are 0.2 and 5 time of measured data.

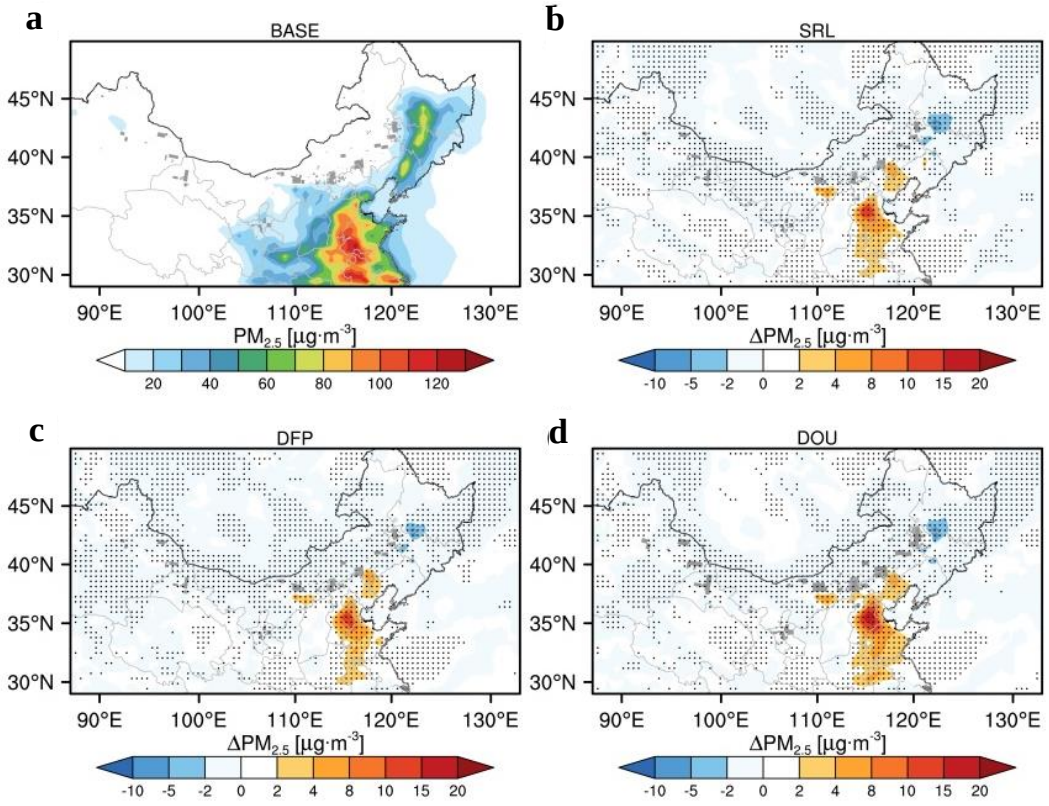

Figure S10. Modelled monthly averaged $PM_{2.5}$ concentration and concentration differences between WFC-related model scenarios and the BASE scenario in January 2016. **(a)** Monthly mean concentration from BASE (S1) simulation; **(b)** $PM_{2.5}$ concentration differences between SRL (S2) and BASE (S1) simulations; **(c)** same as

Fig. S10b but for the differences between DFP (S3) and BASE (S1) simulations; (**d**) same as **Fig. S10b** but for DOU (S4) and BASE (S1) simulations. $PM_{2.5}$ differences are calculated by ($C_{Si} - C_{BASE}$), where C_{Si} denotes modelled concentrations from different model scenarios (i=2, 3, 4). The areas where the monthly $PM_{2.5}$ fractions are significant at the 95% confidence level (*t*-test) are highlighted by the black dots.

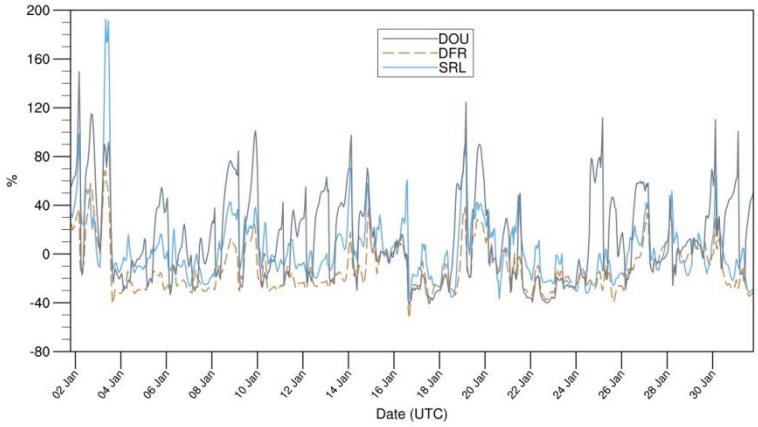

Figure S11. Modeled daily $PM_{2.5}$ concentration fractions (%) in January 2016 from three WFC-related model scenario simulations in Zhangjiakou.

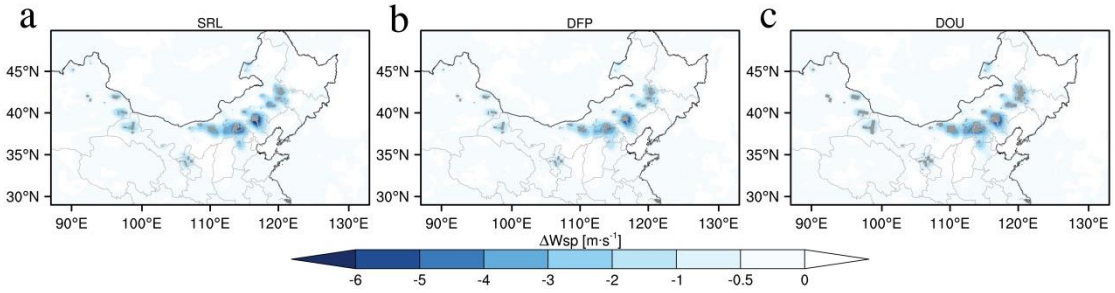

Figure S12. Differences of WRF simulated monthly averaged wind speeds (m s^{-1}) at the hub height from the modeling scenarios SRL (a), DFP (b), and DOU (c) to that from the control (BASE) run in January 2016.

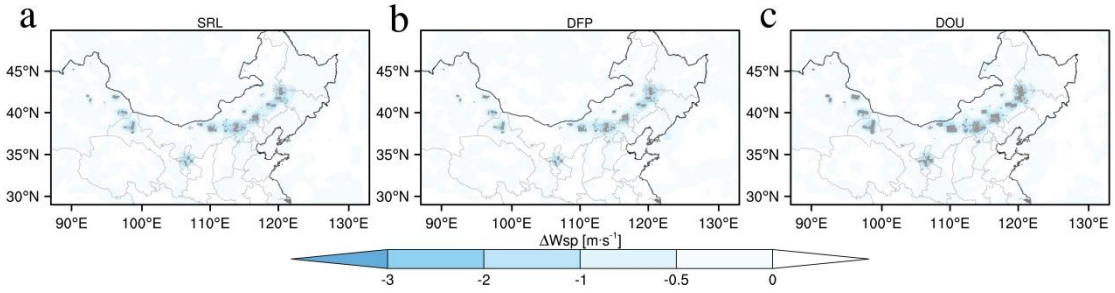

Fig. S13. Same as **Figure S12** but for July 2016.

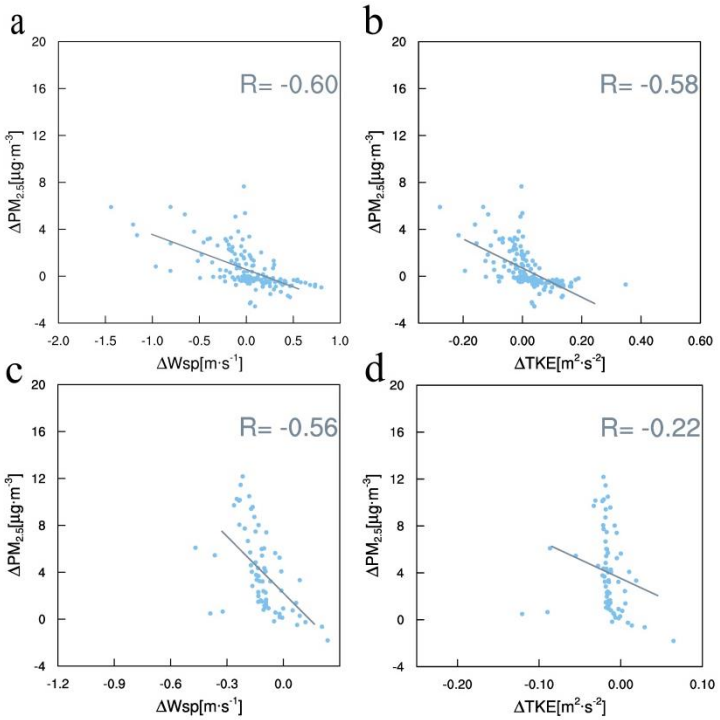

Figure S14. Correlation diagrams of modeled $PM_{2.5}$ differences ($\Delta PM_{2.5}$, μg m^{-3}) and differences of wind speed (ΔV, m s^{-1}) at the hub height and TKE (ΔTKE, m^2 s^{-2}) between DFP and BASE simulations. (a) $\Delta PM_{2.5}$ vs ΔV within WFC in January 2016, (b) $\Delta PM_{2.5}$ vs ΔTKE within WFC in January 2016, (c) $\Delta PM_{2.5}$ vs ΔV in the downstream of WFC in January 2016, (d) $\Delta PM_{2.5}$ vs ΔTKE in the downstream of WFC in January 2016.

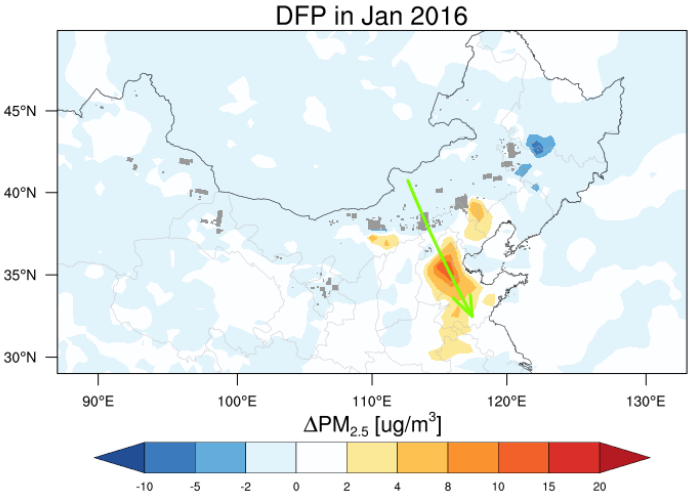

Figure S15. Modeled $\Delta PM_{2.5}$ concentration difference between DFP and BASE simulations averaged over January 2016. The green solid arrow line indicates the transect along which the cross sections of $PM_{2.5}$, TKE, V, and T fractions are generated.

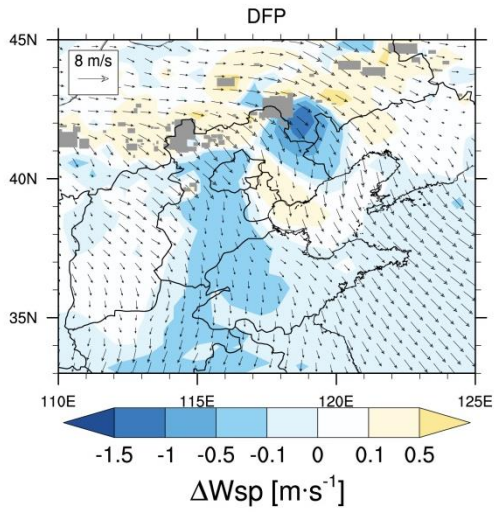

Figure S16. WRF model predicted vector winds (m s^{-1}) and the differences of wind speeds between DFP and BASE model scenario simulations in the model domain in January 2016.

Table S1 WRF-Chem atmospheric physics parameterization schemes adopted in the present study.

Physics options	Scheme
Microphysics	Morrison double-moment scheme (Morrison et al., 2009)
Longwave Radiation	RRTMG scheme (Iacono et al., 2008)
Shortwave Radiation	RRTMG shortwave (Iacono et al., 2008)
Surface Layer	MYNN surface layer (Nakanishi & Niino, 2006)
Land Surface	Noah Land Surface Model
Planetary Boundary layer	MYNN 2.5 level TKE scheme (Nakanishi & Niino, 2006)
Cumulus Parameterization	Grell 3D ensemble scheme (Grell & Dévényi, 2002)

Table S2 Model scenario setup.

scenario	**Scenario setup**
BASE (S1)	no wind farms
SRL (S2)	Wind farms with roughness length scheme
DFP (S3)	Wind farms with drag force scheme
DOU (S4)	Doubling of wind turbines area with drag force scheme

Table S3 Monitoring stations where measured $PM_{2.5}$ air concentration data were collected for model evaluation.

Stations	Beijing	Chengde	Hinggan	Siping	Guyuan
Lat/Lon	N39.972°N, 116.473°E	41.011°N, 117.938°E	46.076°N, 121.946°N	39.788°N, 109.973°E	36.021°N, 106.23°E

Table S4. The statistical metrics between simulated and measured $PM_{2.5}$ air concentrations in monitoring stations (**Table S3**) in January 2016.

Station	Number	R	MB[a]	MGE[a]	NMB[b]	NMGE[b]	FAC2[b]	FAC5[b]	FAC10[b]
Beijing	714	0.52	-4.37	42.72	-6.76	66.19	44.49	89.82	99.30
Chengde	712	0.73	-17.69	17.80	-69.90	70.35	16.32	74.76	96.10
Hinggan	703	0.52	-18.65	18.77	-78.76	79.27	16.60	63.46	89.96
Siping	672	0.70	-0.77	8.58	-4.49	49.95	62.20	91.35	93.58
Guyuan	716	0.78	-24.50	24.80	-54.22	54.89	38.08	90.93	98.05
All stations	3517	0.59	-13.33	22.72	-37.61	64.10	35.54	82.06	95.40

Note: N is the number of sampling hour, R is the linear correlation coefficient, MB is mean bias, NMB the normalised mean bias, MGE the mean gross error, NMGE the normalized mean gross error, FAC2 the fraction of model predictions satisfying: $0.5 \leq Si/Oi \leq 2.0$, where, Si is simulation, Oi is observation, FAC5 is same as FAC2, but for $0.2 \leq Si/Oi \leq 5.0$, FAC10 is same as FAC2, but for $0.1 \leq Si/Oi \leq 10.0$. In these statistical parameters, superscript *a* indicates statistics test for concentration ($\mu g\ m^{-3}$) and *b* is for statistical test for fraction (%).

Table S5. Same as **Table S4** but for July 2016.

Station	Number	R	MB[a]	MGE[a]	NMB[b]	NMGE[b]	FAC2[b]	FAC5[b]	FAC10[b]
Beijing	695	0.22	-2.39	42.30	-3.29	58.32	55.09	88.42	94.56
Chengde	701	0.49	-9.18	24.35	-18.74	49.70	55.09	85.22	93.03
Hinggan	677	0.67	-13.87	14.79	-54.07	57.64	31.80	75.59	86.89
Siping	703	0.40	2.51	14.45	9.85	56.68	61.79	93.86	96.79
Guyuan	703	0.19	-7.95	11.26	-43.50	61.63	42.54	74.62	91.77
All stations	3479	0.59	-6.13	21.43	-16.03	56.10	49.26	83.54	92.61

Table S6. Same as **Table S4** but for air temperatures in January 2016.

Station	Number	R	MB[a]	MGE[a]	NMB[b]	NMGE[b]	FAC2[b]	FAC5[b]	FAC10[b]
Beijing	721	0.86	-5.19	5.29	108.54	-110.65	43.55	78.09	81.83
Chengde	241	0.89	-3.41	3.62	32.92	-34.91	28.99	32.32	32.87
Hinggan	241	0.95	-4.24	4.29	30.03	-30.33	33.15	33.43	33.43
Siping	241	0.95	-2.67	2.73	22.54	-23.06	31.21	32.18	32.18
Guyuan	211	0.79	0.49	2.83	-5.87	-33.63	22.61	26.49	26.77
All	1655	0.87	-3.70	4.21	43.82	-49.88	31.90	40.50	41.42

Table S7. Same as **Table S4** but for air temperatures in July 2016.

Station	Number	R	MB[a]	MGE[a]	NMB[b]	NMGE[b]	FAC2[b]	FAC5[b]	FAC10[b]
Beijing	720	0.82	-0.25	2.47	-0.91	9.04	99.86	99.86	99.86
Chengde	241	0.77	-2.36	3.23	-9.39	12.85	33.43	33.43	33.43
Hinggan	241	0.76	0.22	2.73	0.86	10.51	33.43	33.43	33.43
Siping	241	0.65	2.21	3.19	10.38	14.99	33.43	33.43	33.43
Guyuan	211	0.81	2.37	2.80	14.41	17.03	29.27	29.27	29.27

All	1654	0.81	0.21	2.77	0.84	11.27	45.88	45.88	45.88

Table S8. Same as **Table S4** but for hourly wind speed in January 2016

Station	Number	R	MB[a]	MGE[a]	NMB[b]	NMGE[b]	FAC2[b]	FAC5[b]	FAC10[b]
Beijing	721	0.38	-0.52	1.93	-15.22	56.06	57.84	95.01	97.50
Chengde	231	0.55	2.94	3.01	138.45	141.52	10.26	26.49	30.10
Hinggan	241	0.50	2.54	2.67	87.72	92.06	17.89	32.18	33.29
Siping	234	0.59	1.69	1.85	72.46	79.24	20.25	32.32	32.46
Guyuan	208	0.40	-0.61	1.93	-16.19	51.03	16.78	27.46	28.71
All	1635	0.25	0.73	2.18	23.70	71.23	24.61	42.69	44.41

Table S9. Same as Table S4 but for hourly wind speed in July 2016

Station	Number	R	MB[a]	MGE[a]	NMB[b]	NMGE[b]	FAC2[b]	FAC5[b]	FAC10[b]
Beijing	720	0.21	0.69	1.43	29.90	62.15	65.88	96.81	98.89
Chengde	225	0.17	1.40	1.79	82.16	105.05	15.67	25.52	28.43
Hinggan	236	0.36	1.03	1.48	49.86	71.40	18.17	31.90	32.46
Siping	235	0.11	0.56	1.39	21.39	53.15	22.61	32.18	32.59
Guyuan	210	0.44	-1.51	2.37	-27.78	43.44	20.80	27.60	28.43
All	1626	0.32	0.53	1.60	20.25	60.77	28.63	42.80	44.16

Table S10. Same as Table S8 but for daily wind speed in January 2016

Station	Number	R	MB[a]	MGE[a]	NMB[b]	NMGE[b]	FAC2[b]	FAC5[b]	FAC10[b]
Beijing	30	0.56	-0.55	1.20	-15.79	34.80	90.00	100.00	100.00
Chengde	30	0.85	3.02	3.02	142.73	142.73	23.33	100.00	100.00
Hinggan	30	0.70	2.63	2.63	90.12	90.12	50.00	100.00	100.00
Siping	30	0.80	1.64	1.64	70.40	70.40	66.67	100.00	100.00
Guyuan	30	0.66	-0.72	1.19	-19.01	31.53	86.67	100.00	100.00
All	150	0.27	1.20	1.93	41.26	66.33	63.33	100.00	100.00

Table S11. Same as Table S9 but for daily wind speed in July 2016

Station	Number	R	MB[a]	MGE[a]	NMB[b]	NMGE[b]	FAC2[b]	FAC5[b]	FAC10[b]
Beijing	30	0.23	0.69	0.88	29.86	38.30	83.33	100.00	100.00
Chengde	30	-0.17	1.32	1.39	77.48	81.14	66.67	96.67	100.00
Hinggan	30	0.47	1.00	1.02	48.08	49.11	86.67	100.00	100.00
Siping	30	0.03	0.60	0.89	22.97	34.19	93.33	100.00	100.00
Guyuan	30	0.71	-1.57	1.79	-28.70	32.75	90.00	100.00	100.00
All	150	0.49	0.41	1.19	14.41	42.15	84.00	99.33	100.00

References

Morrison, H., Thompson, G., and Tatarskii, V.: Impact of Cloud Microphysics on the Development of Trailing Stratiform Precipitation in a Simulated Squall Line: Comparison of One- and Two-Moment Schemes, Mon. Weather. Rev., 137, 991-1007, 10.1175/2008mwr2556.1, 2009.

Iacono, M. J., Delamere, J. S., Mlawer, E. J., Shephard, M. W., Clough, S. A., and Collins, W. D.: Radiative forcing by long-lived greenhouse gases: Calculations with the AER radiative transfer models, J. Geophys. Res., 113, D13103, 10.1029/2008jd009944, 2008.

Grell, G. A., and Dévényi, D.: A generalized approach to parameterizing convection combining ensemble and data assimilation techniques, Geophys. Res. Lett., 29, 38-31-38-34, 10.1029/2002gl015311, 2002.

Nakanishi, M., and Niino, H.: An Improved Mellor–Yamada Level-3 Model: Its Numerical Stability and Application to a Regional Prediction of Advection Fog, Bound-lay. Meteorol., 119, 397-407, 10.1007/s10546-005-9030-8, 2006.